Carbon-based piezoresistive polymer composites: Structure and electrical properties

Carbon
Volume 62, October 2013, Pages 270-277
10.1016/j.carbon.2013.05.064

Carbon-based piezoresistive polymer composites: structure and electrical properties

*Sara Cravanzola, Galip Haznedar, Domenica Scarano, Adriano Zecchina and Federico Cesano**

[a] Department of Chemistry, NIS (Nanostructured Interfaces and Surfaces) Centre of Excellence and INSTM Centro di Riferimento, University of Torino, Via P. Giuria, 7, 10125 Torino (Italy);

Abstract

Piezoresistive polymeric composites were prepared by melt mixing of polypropylene (PP) with expanded graphite (EG) (10-15 wt%) and/or multiwalled carbon nanotubes (MWCNTs) (1-2 wt%). The composites were extruded at a temperature of 185°C, by adopting screw speeds in the 2.5-10 rpm range, and fibres with diameters of 0.2, 1.5 and 3 mm, were obtained. An integrated piezoresistive sensor device was obtained by hot pressing the extruded fibres into two sandwiched PP panels.

Structure and morphology of the carbon fillers (EG and MWCNTs) and of the fibres, were investigated by means of X-ray diffraction, optical microscopy, scanning electron microscopy (conventional and conductive SEM) and atomic force microscopy. Piezoelectric properties of fibres and sensor devices were detected through a set up made by a dynamometer, a potentiometer and a digital multimeter. It was shown, that mechanical deformations, due to applied loads, affect remarkably the resistivity of the materials.

*Corresponding author. Tel: +39 0116707834. Fax: +39 0116707855. E-mail address: federico.cesano@unito.it (F. Cesano)

1. Introduction

In recent years, nanostructured hybrid composites have attracted an increasing attention. It is a matter of fact that, by playing with sizes, aspect-ratio, porosity/surface area, energy-gap and composition of nanodomains, many properties of the final material can be suitably tailored, including the catalytic, the electrochemical, the electric, the mechanical, the optical and the magnetic ones [1]. As for the polymer based composites, fillers made by inorganic compounds (i.e. ZnS, SnO_2, ZnO), [2-4] or by carbon based materials (graphene (GR), nanographite (NG), carbon nanofibres (CNFs) or nanotubes (CNTs) [5-9] are of special interest. In fact, depending on the polymer matrix structure and on the peculiar treatments (UV-Vis, γ–ray or moderate temperature curing), the different fillers allow to obtain composites having novel properties [2, 4, 10-12].

More in detail, the excellent electrical and mechanical properties of CNTs make them ideal fillers for making conductive polymer composites. However, there is a limit in the CNTs industrial-scale use, due to their production costs. Otherwise the use of other high aspect-ratio carbon-based fillers (GRs, NGs, etc.) alone or in addition to CNTs could be a good way to improve electrical properties with limited costs.

As for the electric conductivity of CNT/polymer composites, a well detailed description can be made by the percolation theory [13-15]. Following this theory, the material exhibits an abrupt insulator-to-conductor transition at a specific concentration of the conductive filler (percolation threshold), due to the formation of a continuous conductive network. It has been reported, that conductive networks have been recently obtained along segregated paths into the bulk or at the surface of CNT/polymer composites [16, 17], by the laser-stimulated percolation of CNTs [18, 19]. Moreover it is known, that the simultaneous use of different types of conductors (i.e. 1D, 2D and 3D) can help in reducing the electric percolation threshold, as consequence of synergic effects *(vide infra)* [13].

Further interest in CNT/polymer composites comes from their piezoresistive capability, which is strongly dependent on loading type (tension, compression), loading history and then on the matrix mechanical behaviour. This property has been observed in reinforced polymer matrices or wearable textiles [20, 21] as well as in many composites, including carbon nanofibres (CNFs)/PP [22], MWCNT/polyimides (PI), MWCNT/rubbers [23-25] and in hybrid CNTs/EG sheets [26].

Along these themes, MWCNTs/PP, PP/EG and MWCNTs/EG/PP fibres have been investigated with the aim to develop stress-strain sensors to be integrated in composite materials.

2. Materials and methods

2.1 Materials and fabrication of composites

Polypropilene (PP - HIFAX EP3080G, Lyondell Basell, MFI = 11 g/10 min), Expanded Graphite (EG-TIMREX C-THERM001, Timcal) were used as received. Otherwise (1 wt% and 2 wt%) Multiwall Carbon Nanotubes (MWCNTs - Nanocyl NC7000) were obtained from (5% wt) MWCNTs - PP masterbatches.

Polymer fibres and carbon-based composite fibres were prepared according to the following steps: i) melt blending of the raw materials (PP, EG and/or MWCNTs masterbatch) in a mixer with horizontal counter rotating screws (HAAKE PolyLab QC) to obtain homogeneous pellets, ii) extrusion of the composite in a single screw extruder (HAAKE PolyLab QC). Some efforts were made to find more suitable conditions, afterwards the following was selected: a) temperature values: 185°C; b) EG percentages: 5 wt%, 10 wt% and 15 wt%; MWCNTs

percentages: 1 wt% and 2 wt%; c) fibres diameters: 0.2 mm, 1.5 mm and 3 mm; d) screw speeds in the 2,5-10 rpm range.
A sensor device was fabricated via hot pressing (165°C, 100 bar for 5 minutes) of two piezoresistive fibres between two sandwiched PP fabrics 8x4x0.3 cm in size (Propex Curve C100A). For this, fibres 1.5 mm and 3 mm in diameters were chosen, as they can be more easily embedded inside polymer panels or in any devises. (see Supporting Information for details).

2.2 Characterization of materials

2.2.1 Morphology and structure of nanofillers and composites

The morphology of the samples has been investigated by means of: i) Zeiss Evo50 SEM equipped with an energy dispersive X-ray detector (EDAX), ii) AFM (Park Systems XE-100).
Conductivity profiles on cross-sections of the extruded samples were obtained by a secondary electron (SE) detector of a Zeiss Evo50 SEM operating at low acceleration voltage (0.5 KeV). More in details, edge effects on the samples due to secondary-electrons were reduced by working on "flat" sections of the material obtained by means of the ultramicrotome. Specifically, samples, embedded in epoxy resin to fill voids, were then cross sectioned using a regular glass knife. Microtome slices 0.1-1 μm in thickness, representing the cross-section area along the sample length, were obtained [18]. The cross-section slices, contacted on the back sides with conductive Ag paste, were then imaged by low voltage SEM and by conductive AFM as well.
Optical images of cross-section slices were also acquired by Leica DFC290 HD digital camera, integrated with Leica Microsystems' microscopes and LAS (Leica Application Suite) software.
X-Ray Diffraction patterns on samples have been collected with a diffractometer (PANalytical PW3050/60 X'Pert PRO MPD) by using a Ni-filtered Cu anode and working with reflectance Bragg–Brentano geometry for EG and MWCNTs fillers and in the capillary configuration for fibres.

2.2.2 Electrical and piezoelectric properties

Electrical resistance of the samples was measured by using a digital multimeter (Keithley 2420) via two points probe method, whose probes were contacted with Ag conducting electrodes (1 cm apart) to ensure good electrical contacts as well.
In order to perform piezoresistive measurements, the Ag conducting paint was deposited on 24 cm long wires to create two electrodes, 10 cm apart. Mechanical deformations of the samples and the corresponding changes in resistivity were investigated by means of a system constituted of a dynamometer (Instron 5544), a potentiometer and a digital multimeter (Keithley 2700E). The dynamometer, by enabling the application of loads from 0 N to 2000 N, allows to make either traction, flexion and compression tests.
Upon several cycles of mechanical deformation (that is traction of 1 mm, 2 mm and 3 mm of the wires, or flexion of 0.5 mm, 1 mm, 1.5 mm of the panel) the stress-strain curves and the piezoresistive properties of samples were obtained.

3. Results and discussion

3.1 Nanofillers morphology and structure of the extruded materials

The morphology of EG and of MWCNTs fillers is shown in Fig. 1a,b. High aspect ratio EG flakes, ranging in 5-30 μm interval and with domains 25-30 nm in thickness, corresponding to about 60-90 graphene layers, show an irregularly layered structure (Fig. 1a). A dense network of

entangled MWCNTs, 1−5 μm in lengths and 15−20 nm in diameters is shown in Fig. 1b. Due to the high length and flexibility of the MWCNTs nanofilaments, which gives rise to highly interconnected bundles, the percolation threshold can be achieved at low loadings *(vide infra).*

XRD patterns of MWCNTs and of EG flakes, are compared in Fig. 1c. In this figure, the narrow (002) graphite peak, together the weak and broad feature due to MWCNTs, the last one shifting towards smaller diffraction angles, are observed. From this, it results that MWCNTs show a much lower crystallinity, as compared to that of EG flakes.

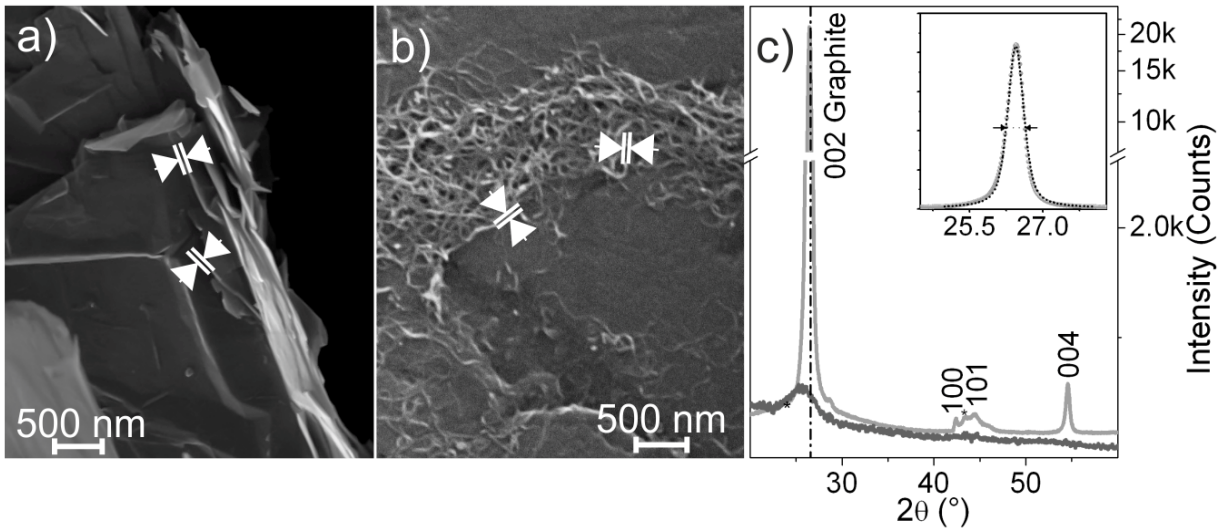

Fig. 1. SEM images of the fillers: a) EG and b) MWCNTs; c) XRD patterns of EG and MWCNTs (gray and black line, respectively). Arrows in a) and b) evidence the thickness of graphite flakes (20-30nm) and the diameters of MWCNTs (~20 nm), respectively. In the inset of c) the (002) XRD diffraction peak of EG in the 2θ = 25-28° range.

Composite fibres, obtained at a temperature of 185°C with an extrusion rate of 2.5-10 rpm. are imaged in Fig. 2a. With the exception of pure PP fibres, all the composite fibres, even containing a low amount of EG or MWCNTs, are completely black.

The XRD patterns of the fibres, shown in fig.2b, show several narrow peaks, assigned to the polymer crystalline phases, emerging from a broad feature, covering the 2θ ≅10-30° range, due to the amorphous phase.

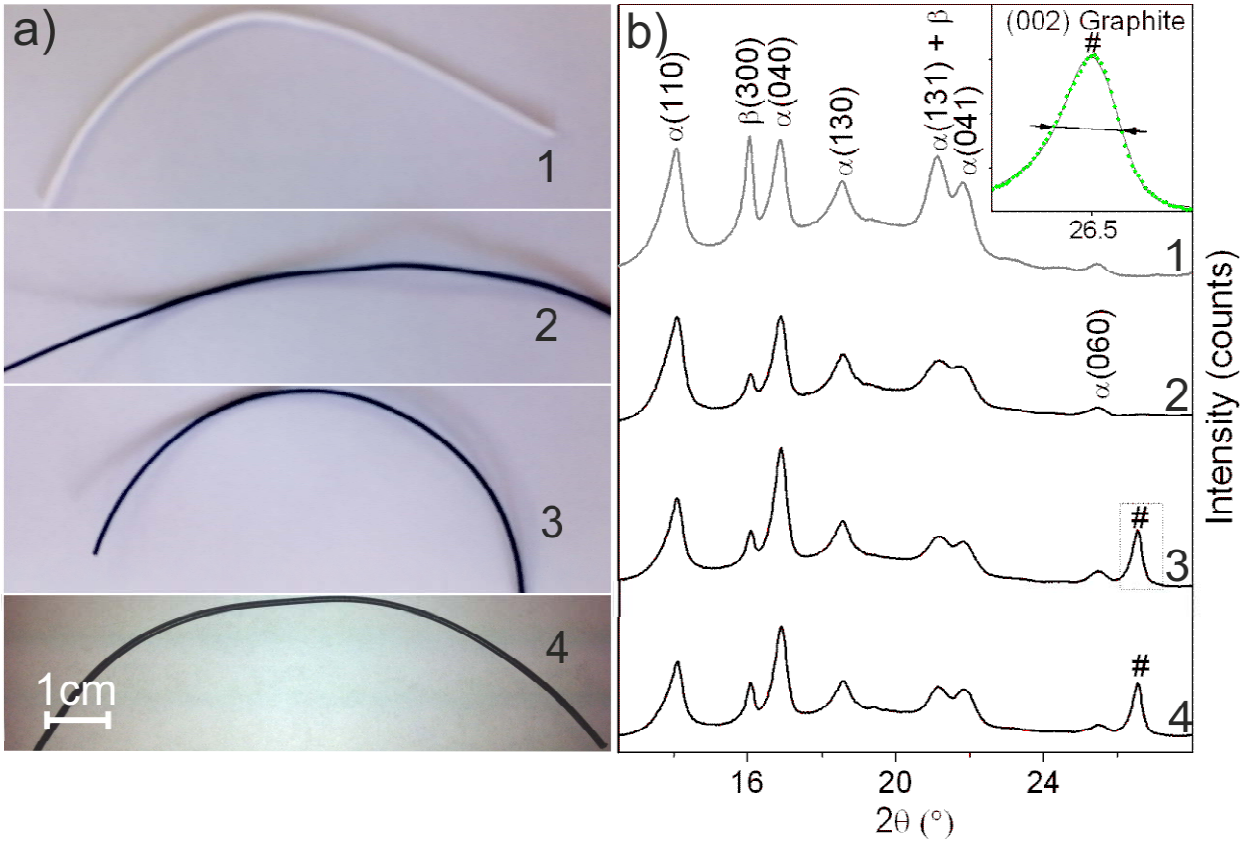

Fig. 2. a) Images and b) XRD diffraction patterns of the extruded fibres, 1.5mm in diameter (extrusion rate = 2.5 rpm) obtained at different compositions: ***1***. Pure PP; ***2***. (2wt%) MWCNT/PP composite; ***3*** (15wt%) EG/PP composite; ***4.*** (2wt%) MWCNT/(15wt%) EG /PP composite.
In the inset of b) enlarged view of the (002) XRD peak in the 2θ ≅ 26-27° range, of (15wt%) EG/PP composite, shown in pattern 3.

The peaks, observed in pattern ***1*** (PP polymer fibre), at 2θ ≅ 14.0°, 16.9°, 18.5°, 25.4°, 28.6°, and at 2θ ≅ 16.0° are ascribed to the α– and β–phases (monoclinic and triclinic) respectively, while those at 2θ≅21.1°and at 2θ ≅ 21.8° are due to the simultaneous presence of both the microcrystalline phases.
Notice that either the 15%wt EG/PP composite (pattern ***3***) and the (2wt%) MWCNT/(15wt%) EG /PP composite (pattern ***4***) show also an additional peak at 2θ ≅ 26.5°, which is associated to the (002) diffraction planes of graphite. Since the XRD peak broadening depends on the coherent scattering domains, by applying the Sherrer's equation to the (002) XRD diffraction peak, it is possible to determine, along the c-axis direction, the thickness of the graphite platelets, embedded inside the composite (enlarged view of pattern ***3*** in the inset of Fig. 2b). A mean value of about 25 nm is obtained, which is quite similar to that obtained for the pure EG (26 nm) (Fig. 1c) in agreement with the SEM analysis.
With Regard to (2wt%) MWCNT/PP composites (pattern ***2***), due to the low quantity (2wt%) and to the poor crystallinity of MWCNTs, no peaks due to crystalline carbon phase were observed. Nevertheless, it is worthy noticing, that the addition of CNTs, even at low concentrations, is affecting the formation of α–PP phase. It is known that the formation of α- and β-PP phases is governed by several parameters, including temperature, heating/cooling rates, pressure, mechanical deformations and the presence of nucleation agents [27], which affect the final

composition. To this regard, it is recognized that the α-PP is the most stable and commonly observed phase, while β-phase (metastable) is usually generated by inclusion of a nucleating agent [28, 29].

3.2 Electrical properties of the samples

Electrical properties of a selection of extruded carbon-based PP composites are reported in Table 1. In particular: a) no conductivity was observed for polymer composite fibres containing only EG percentages lower than 15wt%; b) the same was holding for composites containing less than 2wt% MWCNTs. These are the filler concentrations needed to roughly approach the value of the electric percolation; c) on the contrary fibres containing both the carbon fillers (15wt%EG and 2wt% MWCNTs) showed a conductivity higher than that of the single phases. This is not unexpected, since the peculiar features (i.e. aspect ratio, dimensions, aggregation state) of the conductive phase (s) are known to affect the percolation threshold and hence the conductivity of the composites [8, 16, 30].

To this point, the electric resistances of fibres, containing both EG and MWCNTs (15wt% EG and 2wt% MWCNTs), along and perpendicular to the fibre axis are plotted as a function of the rate of extrusion in Fig 3a. From the obtained data, it appears that the extrusion speed considerably affects the electrical properties of the obtained fibres. In particular, it is observed that, the resistance is increasing, by increasing the extrusion rate. Such behaviour has been attributed to the presence, within the compacted polymer phase, of a segregated structure of carbon nanofillers, which decorate the boundaries between the polymer grains, giving rise to conductive paths. This is in agreement with literature data, revealing ultralow values of percolation threshold in HDPE and UHMWPE composites containing segregated structures of MWCNTs and of GRs [16, 17].

Moreover, the figure shows that, for the same rate of extrusion, larger wires (d=3 mm) have conductivity (lower resistance) higher as compared with the smaller ones (d=1.5 mm) either along and perpendicular to the fibre. Nevertheless, for the same diameters and extrusion rates, the resistance values along the fibres are two orders of magnitude lower than those along the perpendicular directions. An explanation of these findings, which is likely associated with a different distribution of the conductive phases in the polymer matrix, will be discussed later on the basis of SEM and AFM results.

Table 1. Electric resistance* (KΩ) of the extruded polymer composites

	D = 1.5 mm Resistance (KΩ)	**D = 3 mm Resistance (KΩ)**
PP	–	–
PP+ 5wt% EG	–	–
PP+ 10wt% EG	–	–
PP+ 15wt% EG	–	340-14 470 (5-10 rpm)
PP + 1wt% MWCNTs	18 500 000	54 000
PP + 2wt% MWCNTs	5 555 000	15 000
PP + 15wt% EG + 2wt% MWCNTs	≥1 500-2 000 (2.5-3.5 rpm)	59-640 (2.5-10 rpm)

* obtained by two probes analysis. The two electrodes are 1 cm distant.

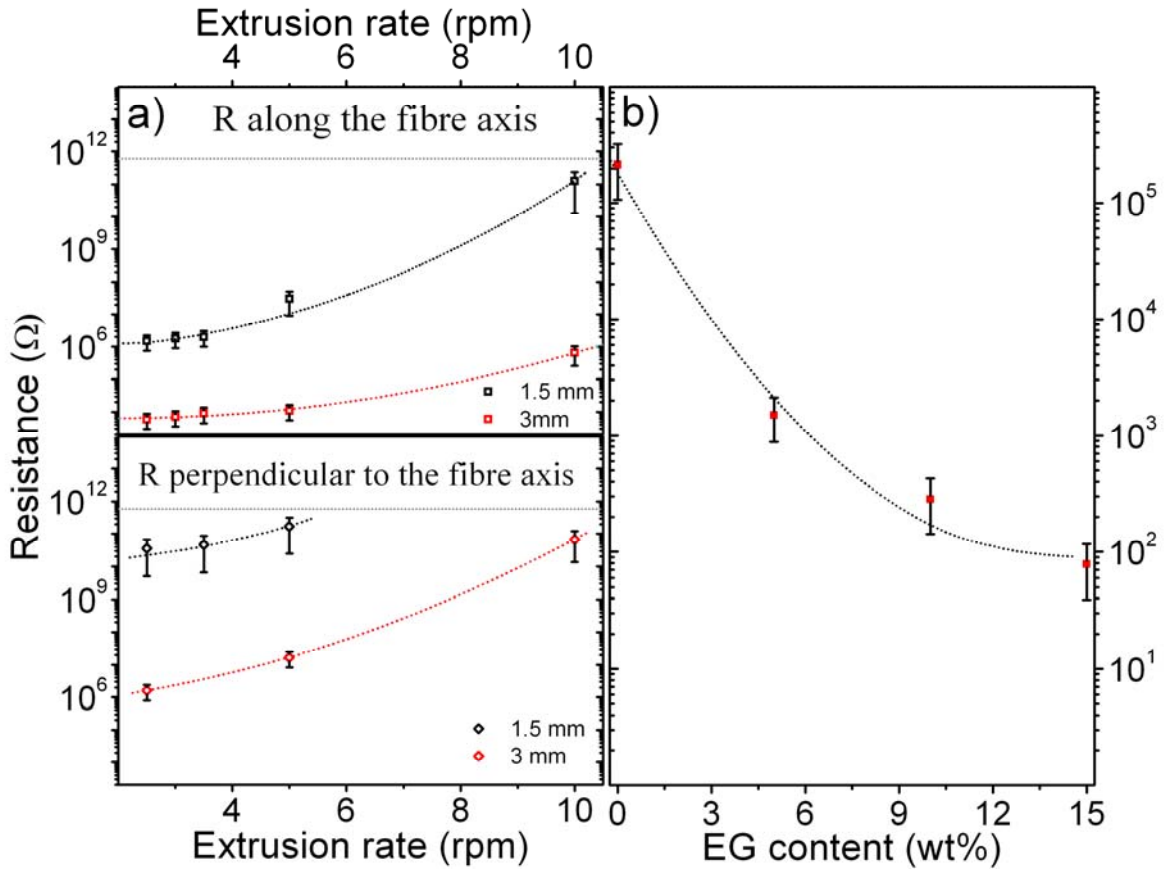

Fig. 3. a) Electrical resistance of the fibres, containing 15 wt% EG and 2 wt% MWCNTs, along (top panel) and perpendicular (bottom panel) to the fibre axis, as function of the extrusion rate (black squares correspond to diameters = 1.5 mm; red squares correspond to diameters = 3 mm). The limit of sensitivity of our electrical measurements is represented by the horizontal black lines in a). The electrical resistance of fibres with d = 1.5 mm, at higher extrusion rate (5 and 10 rpm) exceeds this limit. b) Electrical resistance of flat samples containing a fixed amount of MWCNTs (2%wt) as function of EG content.

Electrical properties of flat PP composites containing a fixed amount of MWCNTs (2wt%) and variable percentages of EG (0-15wt%) are shown in Fig. 3b. From this figure, it is observed that the resistance is decreasing with the EG content; this means that, the combined use of the two types of conducting fillers (MWCNTs and EG) is improving the electric properties. This result can be explained with the synergistic effect, established between the two types of fillers *(see discussion in the next paragraph).*

3.3 Conductive SEM and morphology of the composite fibres

To gain SEM morphological and compositional information, images are usually obtained at high potential (10-30kV). On the contrary, when low acceleration potentials (≈0.1-1kV) are used, the resulting contrast of the imaged areas allows to obtain conductivity surface maps [31]. On this basis, it is evident that SEM data obtained by secondary electrons at low acceleration potential (0.5KV) can be of great help in investigating the distribution of the conducting phases inside the fibers. To check the validity of the method, preliminary acquisitions were obtained on sections of entirely insulating PP fibers, placed on a conductive adhesive tape (Fig. 4a,b,c). The obtained images confirm that, by gradually decreasing the acceleration potential from 5kV to 0.5kV, the

bright regions associated to the insulating material (PP) become dark at lower potentials (~0.75-0.5kV). The principles of this phenomenon (brightness inversion by changing the acceleration potentials in SEM analysis) are well known and discussed in several contributions [31-35].

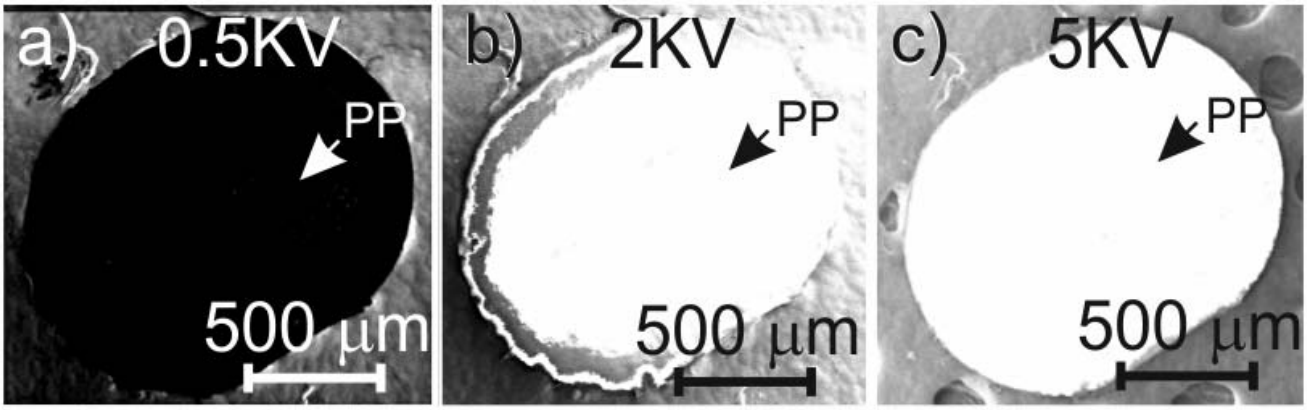

Fig. 4. Low-potential SEM images of slices coming from the extruded polymer, as imaged at different acceleration potentials: a) 0.5kV, b) 2kV and c) 5kV. Notice the brightness inversion of the PP (not conductive at all) image, by changing the acceleration potentials, when compared to the conductive adhesive surrounding the polymer slice.

SEM conductivity maps obtained at low potentials on sections of composite fibres are shown in Fig. 5a-d. From these images, the dark regions correspond to insulating areas, while the white regions correspond to highly conductive areas.

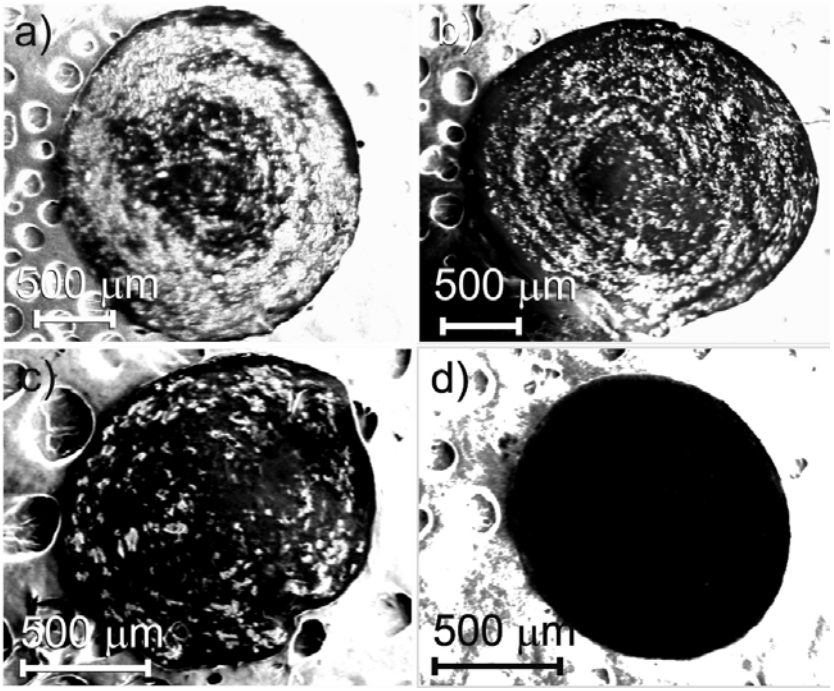

Fig. 5. Low-potential (0.5kV) SEM images of fibre cross sections (constituted of 15wt% EG and 2wt% MWCNTs), obtained at: a) 5 rpm and b) 10 rpm (fibres 3 mm in diameter), c) 5rpm and d) 10 rpm (fibres 1.5 mm in diameter).

More in details, the following can be observed: a) for a selected diameter of the fibre, the size of the bright regions decrease with increasing of the extrusion rate; ii) the same happen for a specific extrusion rate moving from smaller to larger diameters, iii) the fibres with the smallest diameters obtained at low extrusion rate show very localized conductive regions, which are

substantially identical for all samples, iv) low diameter fibres extruded at high speed don't show white regions and hence they are not conductive. All these observations are fully consistent with the electrical measurements reported in Fig. 3. From these results, it can be highlighted that the extrusion rates have a relevant role in affecting the aggregation of the conductive filler particles. In particular at low extrusion rates, the aggregation/segregation of the filler particles along the grain boundaries is highly favoured with formation of conductive pathways within the polymeric matrix, being this behaviour plausibly associated with more easy diffusion mechanisms.
Two regions of a fibre cross-section, 1.5 mm in size, obtained under 5 rpm extrusion rate and containing 15wt% EG and 2wt% MWCNTs, , are SEM and AFM imaged in Fig. 6a and 6b.

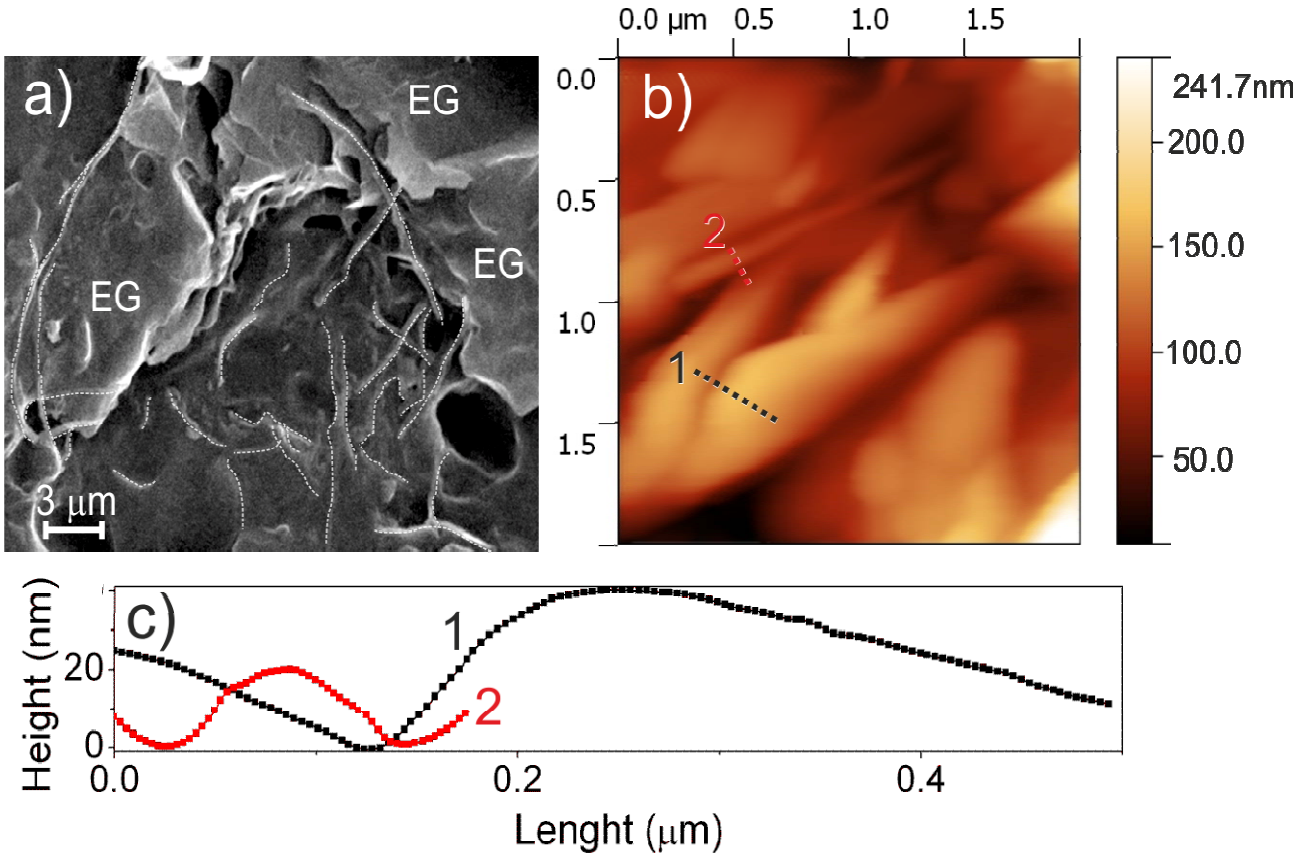

Fig. 6. SEM and AFM imaging of a conductive composite fibre containing 15wt% EG and 2wt% MWCNTs (extrusion rate =5 rpm, d=1.5mm): a) SEM image of a conductive region, where dotted lines indicate MWCNTs pathways; b) nc-AFM image of 2x2 µm region; c) height profiles along the selected lines drawn in b).

In fig 6a the presence of MWCNTs through the polymer matrix is highlighted by the pathways shown by dotted lines, which, by establishing connections with EG, create a dense network.
The AFM image (Fig. 6b) of a selected conductive area in more internal regions evidences clearly graphite planes (40 nm thick), connected with a MWCNT protruding from the polymer rounded particles. The height profiles shown in Fig. 6c confirm this interpretation. The co-presence of phases, containing conductive fillers of different dimensionality (i.e. 1D and 2D), in agreement with the SEM image of isolated conductive areas, provides with one plausible explanation of the enhancement in conductivity of the composite. This effect, known as *synergistic effect*, has been also observed in polymer composites containing carbon black and

CNTs [36, 37], EG and CNTs [38]. In particular, it is known that flexible 1D CNTs, beside the segregated structures around polymer grains, can promote the formation of new paths by bridging adjacent 2D graphite platelets, thus generating conductive architectures, as imaged in Fig. 6a and b. According to this model, stacking of bidimensional EG is inhibited in presence of one-dimensional MWCNTs, which causes high contact areas and steric/electrostatic stabilization between fillers and polymer matrix. On this basis the observed dispersions in Fig. 6a and b can found an explanation. In conclusion, either segregation phenomena due to MWCNTs either synergistic effects of both fillers affect in a remarkable way the conductivity.
It has been also demonstrated that the synergy between different carbon phases in polymers enhance other properties (e.g. mechanical properties) [39].

3.4 Piezoresistive properties

Piezoresistive properties of a conductive fibre (d =1.5 mm, containing 15wt% EG and 2wt% MWCNTs) were obtained upon cyclic moderate elongations (ε=0.4%, 0.8% and 1.2%, respectively). The relative variations in electric resistance (R/R_0) and the elongation cycles are reported in Fig. 7a,b, respectively.
Piezoresistive properties were also obtained for the same fibre inserted into two PP panels (8x4x 0.3cm in size, see Supporting Information). The panels are used as a three point flexural test of an embedded flexure sensor. The variations in electric resistance (R/R_0) and the deflections (0.5 mm, 1 mm and 1.5 mm) of the composite sandwich are reported in Fig. 7d-e, respectively.

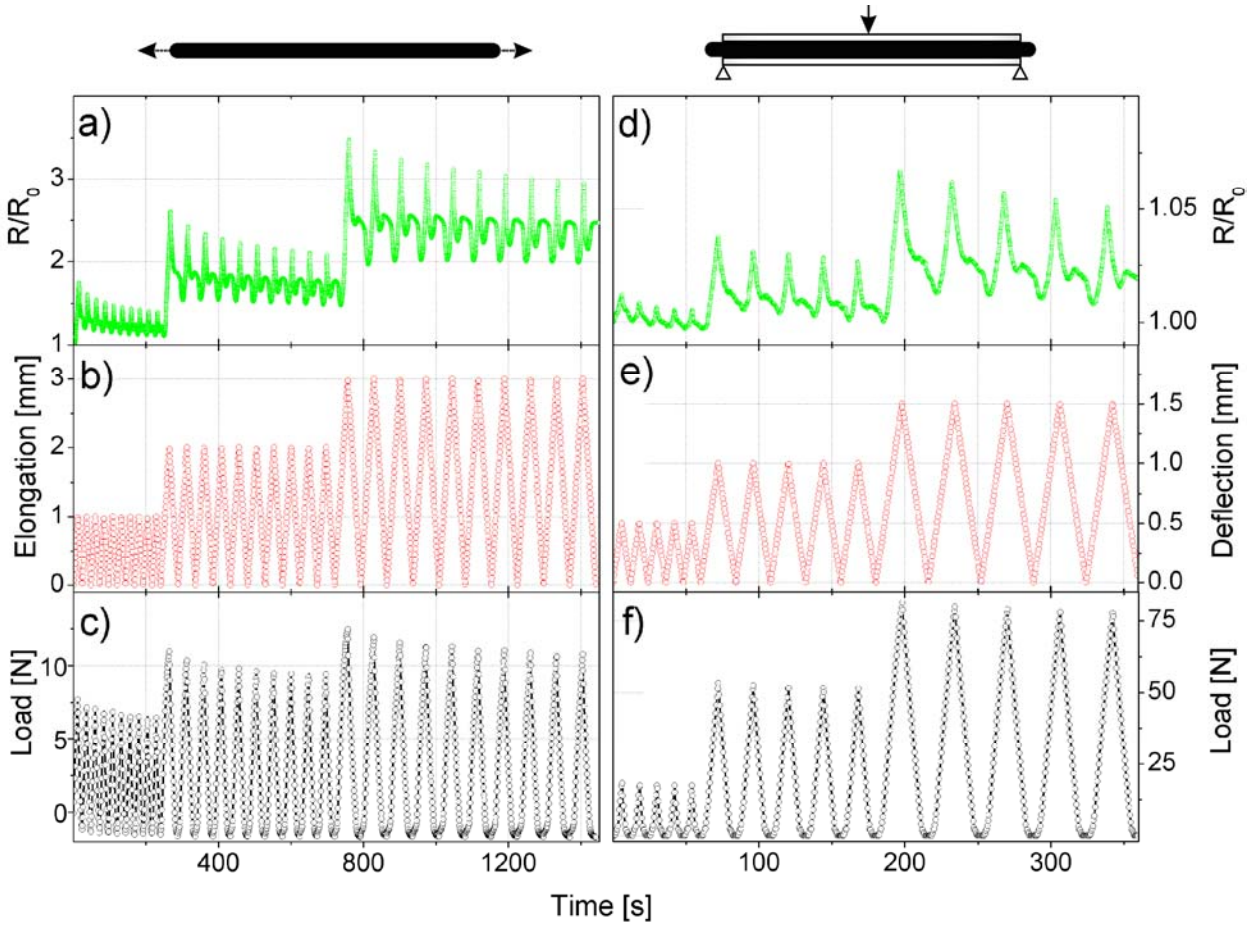

Fig. 7. a) and d) Piezoresistive variations (R/R_0) of the composite fibre (15wt% of EG and 2wt% of MWCNTs in PP, obtained under 2.5 rpm extrusion rate) upon tensile loading (left panels) and

upon three point flexure tests after embedding in PP panels (rights panels); b) and e) cyclic deformations (elongation of the fibre and deflection of the composite panels); c) and f) loading cycles, for elongations and deflections, respectively.

The full description of the piezoresistive process goes beyond the scope of this work, nevertheless to explain the non-specular signal in loading/unloading cycles, some considerations can be drawn. First of all, for piezoresistive CNT-based polymer composites a linear piezoresistivity is usually obtained under low strains ($\varepsilon < 1\%$), followed by non linearity at larger strains [30].

It is inferred that under repeated elongations of the fibre, R/R_0 slightly drifts downward, but abruptly increases for increased loadings (Fig. 7 left panels). In other words, the R/R_0 changes are proportional to the tensile stress with synchronous variations and a good signal/noise ratio.

In particular, the small reduction of the R/R_0 amplitude, observed under a high number of cycles for each elongation percentage, may be explained with rearrangements of the CNTs network due to the viscoelastic nature of the matrix. After each cycle, R/R_0 does not go back to its initial value, indicating that phenomena occurring in the polymer matrix permanently modify the morphology of the CNTs network. Moreover, higher elongations induced by higher loadings are affecting more deeply the strain accumulated in the polymer matrix, thus explaining the observed abrupt rise of R/R_0 [40]. From this a relation between piezoresistive effects and stress/strain can be shown.

We come to similar conclusions by making piezoresistive test on the composite sandwich (Fig. 7 right panels), although R/R_0 values depend on the different experimental conditions adopted for the flexure test.

In addition, at the end of each cycle, after the release of the stress, a rebound peak of R/R_0 is observed. A similar effect has been discussed in carbon polymer composite fibres upon cyclic tension or cyclic tension-compression. Bumps, occurring in return steps, were ascribed to the fiber buckling, thus causing the straightness degree to decrease and the resistivity to increase reversibly [41]. Since the electric conductivity of the nanocomposites is deeply affected from aggregation phenomena, it comes that variations of conductive networks due to loss of contacts among nanofillers upon deformation and the intrinsic piezoresistivity of MWCNTs and of EG flakes can be inferred. However, the electric conductivity in conductive polymer composites above the percolation threshold is a complex phenomenon, which can be also explained with tunnelling effects among neighbouring EG flakes and/or MWCNTs nanofillers.

The mechanical and piezoresistive stability of the composite has been tested through a cyclic tensile-loading test (elongations of 1 mm for 100 cycles). Results are shown in the supplementary data. It can be briefly summarized that after few cycles the R/R_0 values stabilize around $R/R_0 = 1$, being the same behaviour observed for the loading-unloading curves. This means that the modifications of the electrical resistance occurring during loading-unloading cycles are correlated to matrix mechanical behavior, that is phenomena such as yielding and deformations, affecting the filler network inside the polymer matrix [40].

4. Conclusions

A piezoresistive sensor device has been made by integrating two piezoresistive fibres into two sandwiched PP panels. Each conductive fibre inside the devise is able to monitor different areas of the panel. By monitoring the changes in electrical resistance of each fibre compared to the initial value, it is possible to evaluate the role of an applied load in affecting the mechanical

properties of a portion of the panel. In our specific case, during the tests, we obtained decreased values of electrical resistance. Actually, we have shown that, to evaluate the structural integrity of a material, it's enough to examine the electrical resistance as function of the time, without analysing the stress-strain curves.

References

[1] Rao CNR, Müller A, Cheetham AK, eds. The Chemistry of Nanomaterials: Synthesis, Properties and Applications. Weinheim, FRG.: Wiley-VCH Verlag GmbH & Co. KGaA 2005.

[2] Lü C, Cheng Y, Liu Y, Liu F, Yang B. A Facile Route to ZnS–Polymer Nanocomposite Optical Materials with High Nanophase Content via gamma-Ray Irradiation Initiated Bulk Polymerization. Advanced Materials. 2006;18(9):1188–92.

[3] Rahman MM, Cesano F, Bardelli F, Scarano D, Zecchina A. Hybrid SnO_2/carbon composites: From foams to films by playing with the reaction conditions. Catalysis Today. 2010;150(1):84-90.

[4] Cesano F, Bertarione S, Damin A, Agostini G, Usseglio S, Vitillo JG, et al. Oriented TiO_2 nanostructured pillar arrays: Synthesis and characterization. Advanced Materials. 2008;20(17):3342-8.

[5] Ci L, Suhr J, Pushparaj V, Zhang X, Ajayan PM. Continuous Carbon Nanotube Reinforced Composites. Nano Letters. 2008; 8(9):2762-6.

[6] Du J, Cheng H-M. The Fabrication, Properties, and Uses of Graphene/Polymer Composites. Macromolecular Chemistry and Physics. 2012;213(10-11):1060−77.

[7] Lin W, Zhang R, Wong CP. Modeling of Thermal Conductivity of Graphite Nanosheet Composites. Journal of Electronic Materials. 2010;39(3):268-72.

[8] Potts JR, Dreyer DR, Bielawski CW, Ruoff RS. Graphene-based polymer nanocomposites. Polymer. 2011;52:5-25.

[9] Cesano F, Bertarione S, Scarano D, Zecchina A. Connecting carbon fibers by means of catalytically grown nanofilaments: Formation of carbon-carbon composites. Chemistry of Materials. 2005;17(20):5119-23.

[10] Tsitsilianis C, Gotzamanis G, Iatridi Z. Design of "smart" segmented polymers by incorporating random copolymers as building blocks. European Polymer Journal. 2010;47(4):497–510.

[11] Cesano F, Pellerej D, Scarano D, Ricchiardi G, Zecchina A. Radially organized pillars of TiO_2 nanoparticles: synthesis, characterization and photocatalytic tests. Journal of Photochemistry and Photobiology a-Chemistry. 2012;242:51-8.

[12] Ha HJ, Kwon YH, Kim JY, Lee S-Y. A self-standing, UV-cured polymer networks-reinforced plastic crystal composite electrolyte for a lithium-ion battery. Electrochimica Acta. 2011;57:40-5.

[13] Zhang W, Dehghani-Sanij AA, Blackburn RS. Carbon based conductive polymer composites. Journal of Materials Science. 2007;42(10):3408-18.

[14] Kaiser AB, Skakalova V. Electronic conduction in polymers, carbon nanotubes and graphene. Chemical Society Reviews. 2011;40(7):3786-801.

[15] Sanjinés R, Abad MD, Vâju C, Smajda R, Mionić M, Magrez A. Electrical properties and applications of carbon based nanocomposite materials: An overview. Surf Coat Tech. 2011;206:727-33.

[16] Du J, Zhao L, Zeng Y, Zhang L, Li F, Liu P, et al. Comparison of electrical properties

between multi-walled carbon nanotube and graphene nanosheet/high density polyethylene composites with a segregated network structure. Carbon. 2011;49(4):1094-100.
[17] Hu H, Zhang G, Xiao L, Wang H, Zhang Q, Zhao Z. Preparation and electrical conductivity of graphene/ultrahigh molecular weight polyethylene composites with a segregated structure. Carbon. 2012;50(12):4596-9.
[18] Cesano F, Rattalino I, Demarchi D, Bardelli F, Sanginario A, Gianturco A, et al. Structure and properties of metal-free conductive tracks on polyethylene/multiwalled carbon nanotube composites as obtained by laser stimulated percolation. Carbon. 2013;In Press (DOI:10.1016/j.carbon.2013.04.066).
[19] Gao W, Singh N, Song L, Liu Z, Reddy ALM, Ci L, et al. Direct laser writing of micro-supercapacitors on hydrated graphite oxide films. Nature Nanotech. 2011;6(8):496-500.
[20] Loyola BR, La Saponara V, Loh KJ. In situ strain monitoring of fiber-reinforced polymers using embedded piezoresistive nanocomposites. Journal of Materials Science. 2010;45:6786-98.
[21] Huang C-T, Shen C-L, Tang CF, Chang SH. A wearable yarn-based piezo-resistive sensor. Sensor Actuat A-Phys. 2008;141:396-403.
[22] Rocha JG, Paleo AJ, Hattum FWJv, Lanceros-Méndez S. Piezoresistive polypropylene-carbon nanofiber composites as mechanical transducers. Microsyst Technol. 2012;18(5):591-7.
[23] Gau C, Ko SH, Chen HT. Piezoresistive characteristics of MWCNT nanocomposites and fabrication as a polymer pressure sensor. Nanotechnology. 2009;20(18):185503(1-11).
[24] Obitayo W, Liu T. A Review: Carbon Nanotube-Based Piezoresistive Strain Sensors. Journal of Sensors. 2012;2012:652438(1-15).
[25] Dang Z-M, Jiang M-J, Xie D, Yao S-H, Zhang L-Q, Bai J. Supersensitive linear piezoresistive property in carbon nanotubes/silicone rubber nanocomposites. J Appl Phys. 2008;104(2):024114(1-6).
[26] Hwang S-H, Park H, Park Y-B. Piezoresistive behavior and multi-directional strain sensing ability of carbon nanotube–graphene nanoplatelet hybrid sheets. Smart Mater Struct. 2013; 22 015013.
[27] Tordjeman P, Robert C, Marin G, Gerard P. The effect of α, β crystalline structure on the mechanical properties of polypropylene. Eur Phys J E. 2001;4(4):459–65.
[28] Bikiaris D. Microstructure and Properties of Polypropylene/Carbon Nanotube Nanocomposites. Materials 2010;3(4):2884.
[29] Bhattacharyya AR, Sreekumar TV, Liu T, Kumar S, Ericson LM, Hauge RH, et al. Crystallization and orientation studies in polypropylene/single wall carbon nanotube composite. Polymer. 2003;44(8):2373-7.
[30] Alamusi NH, Hisao F, Satoshi A, Yaolu L, Jinhua L. Piezoresistive Strain Sensors Made from Carbon Nanotubes Based Polymer Nanocomposites. Sensor. 2011;11(11):10691-723.
[31] Li W, Bauhofer W. Imaging of CNTs in a polymer matrix at low accelerating voltages using a SEM. Carbon. 2011;49(12):3891-8.
[32] Li W, Buschhorn ST, Schulte K, Bauhofer W. The imaging mechanism, imaging depth, and parameters influencing the visibility of carbon nanotubes in a polymer matrix using a SEM. Carbon. 2011;49(6):1955-64.
[33] Loos J, Alexeev A, Grossiord N, Koning CE, Regev O. Visualization of single-wall carbon nanotube (SWNT) networks in conductive polystyrene nanocomposites by charge contrast imaging. Ultramicroscopy. 2005;104(2):160-7.

[34] Jayakody GH, Wells TRC, El-Gom MM. Imaging of doped Si in low and very low voltage SEM: the contrast interpretation. Journal of Electron Spectroscopy and Related Phenomena. 2005;143(2-3):233–9.
[35] Ura K, Aoyagi S. Static capacitance contrast of LSI covered with an insulator film in low accelerating voltage scanning electron microscope. Journal of Electron Microscopy. 2000;49(1):157-62.
[36] Zhang SM, Lin L, Deng H, Gao X, Bilotti E, Peijs T, et al. Synergistic effect in conductive networks constructed with carbon nanofillers in different dimensions. Express Polymer Letters. 2012 Feb;6(2):159-68.
[37] Wen M, Sun X, Su L, Shen J, Li J, Guo S. The electrical conductivity of carbon nanotube/carbon black/polypropylene composites prepared through multistage stretching extrusion. Polymer. 2012;53(7):1602-10.
[38] Kostagiannakopoulou C, Maroutsos G, Sotiriadis G, Vavouliotis A, Kostopoulos V. Study on the synergistic effects of graphene/carbon nanotubes polymer nanocomposites. Proc SPIE. 2011;8409:840911.
[39] Prasad KE, Das B, Maitra U, Ramamurty U, Rao CNR. Extraordinary synergy in the mechanical properties of polymer matrix composites reinforced with 2 nanocarbons. PNAS. 2009;106(32):13186–9.
[40] Ku-Herrera JJ, Aviles F. Cyclic tension and compression piezoresistivity of carbon nanotube/vinyl ester composites in the elastic and plastic regimes. Carbon. 2012;50(7):2592-8.
[41] Shui X, Chung DDL. A piezoresistive carbon filament polymer-matrix composite strain sensor. Smart Mater Struct. 1996;5(2):243-6.

Supplementary Data

Carbon-based piezoresistive polymer composites: structure and electrical properties

Sara Cravanzola, Galip Haznedar, Domenica Scarano, Adriano Zecchina and Federico Cesano[2]

[a] Department of Chemistry, NIS (Nanostructured Interfaces and Surfaces) Centre of Excellence and INSTM Centro di Riferimento, University of Torino, Via P. Giuria, 7, 10125 Torino (Italy);

Supplementary Data

Polypropylene panel with an embedded piezorestive fibre (15wt% of EG and 2wt% of MWCNTs in PP) of 1.5 mm in diameter, working as stress-strain sensor

Pictures of the polypropylene fabric, and of the obtained sandwiched composite panel are shown in Figure S1.

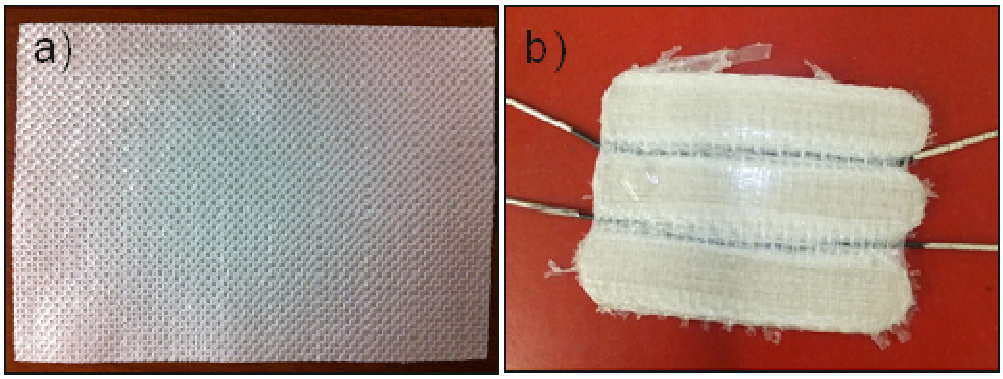

Figure S1. Images of the polypropylene fabric a) and of the sandwiched composite b).

[2]Corresponding author. Tel: +39 0116707854. Fax: +39 0116707855. E-mail address: federico.cesano@unito.it (F. Cesano).

Piezoresitive changes and mechanical stability during tensile-loading tests for 1mm elongation during 100 cycles

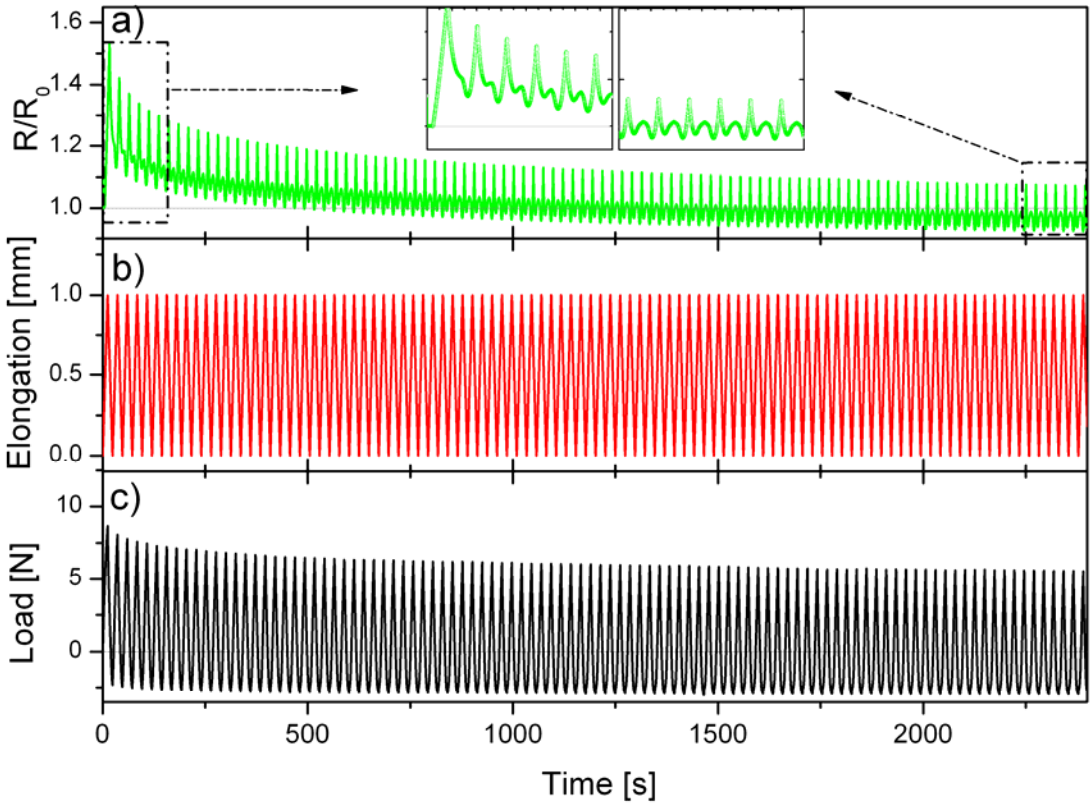

Figure S2. a) Piezoresistivity (R/R_0), b) 100 cycles sequence of 1 mm elongation, c) tensile-loading tests and mechanical stability of the conductive polymer composite fibre (d=1.5 mm). The phase composition of the fibre is the same than that adopted for the piezoresistive tests reported in Fig. 7 (15wt% of EG and 2wt% of MWCNTs in PP, obtained under 2.5 rpm extrusion rate). In the insets of a) R/R_0 variations during the initial and final cycles are shown.